Mineralium Deposita (2018) 53:1061–1078
https://doi.org/10.1007/s00126-017-0790-0

ARTICLE

Subsurface deposition of Cu-rich massive sulphide underneath a Palaeoproterozoic seafloor hydrothermal system—the Red Bore prospect, Western Australia

Andrea Agangi[1] · S. M. Reddy[1] · D. Plavsa[1] · C. Vieru[2] · V. Selvaraja[3] · C. LaFlamme[3] · H. Jeon[4] · L. Martin[4] · T. Nozaki[5] · Y. Takaya[6] · K. Suzuki[5]

Received: 30 January 2017 / Accepted: 27 December 2017 / Published online: 1 February 2018

Abstract

The Proterozoic Bryah and Yerrida basins of Western Australia contain important base and precious metal deposits. Here we present microtextural data, trace element and S isotope analyses of massive sulphide mineralisation hosted in Palaeoproterozoic subvolcanic rocks (dolerite) recently discovered at Red Bore. The small-scale high-grade mineralisation, which extends from the sub-surface to at least 95 m down-hole, is dominated by massive chalcopyrite and contains minor pyrite and Bi-Te-(Se) phases. Massive sulphide mineralisation is surrounded by discontinuous brecciated massive magnetite, and a narrow (< 2 m) alteration halo, which suggests very focussed fluid flow. Laser ablation ICP-MS analyses indicate that chalcopyrite contains up to 10 ppm Au and in excess of 100 ppm Ag. Sulphur isotope analyses of pyrite and chalcopyrite indicate a narrow range of $\delta^{34}S_{VCD}$ (− 0.2 to + 4.6 ‰), and no significant mass-independent fractionation ($-0.1 < \Delta^{33}S < +0.05$ ‰). Re-Os isotope analyses yield scattered values, which suggests secondary remobilisation. Despite the geographical proximity and the common Cu-Au-Ag association, the mineralisation at Red Bore has significant differences with massive sulphide mineralisation at neighbouring DeGrussa, as well as other massive sulphide deposits around the world. These differences include the geometry, sub-volcanic host rocks, extreme Cu enrichment and narrow $\delta^{34}S$ ranges. Although a possible explanation for some of these characteristics is leaching of S and metals from the surrounding volcanic rocks, we favour formation as a result of the release of a magmatic fluid phase along very focussed pathways, and we propose that mixing of this fluid with circulating sea water contributed to sea floor mineralisation similar to neighbouring VHMS deposits. Our data are permissive of a genetic association of Red Bore mineralisation with VHMS deposits nearby, thus suggesting a direct connection between magmatism and mineralising fluids responsible for VHMS deposition at surface. Therefore, the Red Bore mineralisation may represent the magmatic roots of a VHMS system.

Editorial handling: D. Huston

Electronic supplementary material The online version of this article (https://doi.org/10.1007/s00126-017-0790-0) contains supplementary material, which is available to authorized users.

✉ Andrea Agangi
aagangi@uj.ac.za

[1] Department of Applied Geology, Curtin University, Bentley, WA 6012, Australia

[2] Thundelarra Ltd., 186 Hampden Road, Nedlands, WA 6009, Australia

[3] Centre for Exploration Targeting (CET), University of Western Australia, 35 Stirling Highway, Crawley, WA 6009, Australia

[4] Centre for Microscopy, Characterisation and Analysis (CMCA), University of Western Australia, 35 Stirling Highway, Crawley, WA 6009, Australia

[5] Research and Development (R&D) Center for Submarine Resources, Japan Agency for Marine-Earth Science and Technology (JAMSTEC), 2-15 Natsushima-cho, Yokosuka, Kanagawa 237-0061, Japan

[6] Department of Resources and Environmental Engineering, School of Creative Science and Engineering, Waseda University, 3-4-1 Okubo, Shinjuku-ku, Tokyo 169-8555, Japan

Introduction

Volcanic-hosted massive sulphide (VHMS) deposits are the source of significant amounts of Cu, Zn, Pb, Ag and Au (Large 1992; Galley et al. 2007). These deposits form in submarine environments, at both extensional and convergent margin settings (Yeats et al. 2014; Huston et al. 2010; Galley et al. 2007; Binns et al. 2007), where convective sea water circulation, driven by magma intrusion at shallow crustal depths, deposits metals when these heated fluids are discharged back into sea water (Ohmoto 1996; Ross and Mercier-Langevin 2014). VHMS deposits occur discontinuously throughout Earth's history from the Archaean to the Phanerozoic (Huston et al. 2010; Sharpe and Gemmell 2002) and are considered to be the fossilised equivalents of present day massive sulphides deposited at the emergence of submarine hydrothermal systems (de Ronde et al. 2005; Hannington 2014; Petersen et al. 2014).

This mechanism of ore deposition implies two end members for the source of metals: the country rocks (including sediments, volcanic rocks and the basement) and the magma that drives convective circulation. The leaching of country rocks by circulating sea water is a widely accepted mechanism as a source of metals, for example in Kuroko-type VHMS deposits (Ohmoto 1996). More recently, substantial evidence has emerged pointing to a significant magmatic contribution for both fluids and metals in ancient and present day systems (Huston et al. 2011; Moss et al. 2001; Gemmell et al. 2004). Sea water involvement in the deposition of VHMS mineralisation is indicated by (1) low, sea water-like salinity of fluid inclusions (5–6 wt% Na_{eq} on average; Peter et al. 2007), although high-salinity brines and vapours have been observed in some modern vents and ancient VHMS deposits (Shanks III 2001; Solomon et al. 2004), likely due to phase separation; (2) $\delta^{18}O$ (> 5‰) and $\delta^{34}S$ of sulphate minerals indicating equilibrium with sea water at the time of deposition (de Ronde et al. 2014); 3) O and H isotope composition of alteration minerals associated with sea water interaction with hot magmatic rocks (Shanks III 2001; Shanks III 2012) and of fluids emitted at present-day submarine centres (de Ronde et al. 2005); and 4) in the specific case of Archaean VHMS deposits, multiple S isotope signatures of sulphide minerals yielding $\Delta^{33}S < 0$, implying sourcing of S from Archaean sea water sulphate (Farquhar et al. 2011; Bekker et al. 2009; Chen et al. 2015). On the other hand, studies of volcanic rocks associated with VHMS deposits (Timm et al. 2012; Moss et al. 2001) and melt inclusions in unmineralised rocks from the Manus basin (Kamenetsky et al. 2001; Yang and Scott 1996) have shown that magmas are potential sources of metals in this type of deposits. A magmatic involvement is expected to be reflected in geochemical and isotopic compositions of some VHMS deposits, such as enrichment of Cu-Au-Ag-Bi-Se, intermediate to high-sulfidation assemblages, high fluid $\delta^{18}O$, narrow $\delta^{34}S$ ranges and aluminous alteration (Peter et al. 2007; Huston et al. 2011). However, it is difficult to determine whether these observations are the result of magmatic-hydrothermal fluid input or leaching of volcanic rocks by sea water-derived fluids.

Here, we present textural and mineralogical observations, trace element and S isotope compositions of recently discovered mineralisation, called the Red Bore prospect of central Western Australia (Fig. 1) and evaluate its formation in the light of the previous discussion. This mineralisation includes pipe-like massive chalcopyrite ore spatially related to VHMS deposits hosted in a Palaeoproterozoic mafic volcanic succession. The geometry and the very Cu-rich composition set this mineralisation apart from VHMS mineralisation at the district scale.

Geological setting

Regional geology

Sulphide mineralisation at Red Bore is hosted by the mafic igneous rocks of the Narracoota Formation within the Bryah Basin (Fig. 1). The volcano-sedimentary Bryah and Padbury Groups were deposited along the northern margin of the Yilgarn Craton between 2000 and 1800 Ma (Occhipinti et al. 1998, 2004; Pirajno and Occhipinti 2000) and are interpreted to have formed on a continental margin or in a rift setting (Occhipinti et al. 1998; Pirajno et al. 2004; Pirajno and Occhipinti 2000). A recent model proposed that extension was preceded by upwelling caused by the impingement of a mantle plume (Pirajno et al. 2016). The Karalundi Formation is the lowest unit of the Bryah Basin and includes a clastic sedimentary succession (conglomerate, wacke, siltstone, black shale) and mafic volcanic rocks (Pirajno and Occhipinti 2000). The Narracoota Formation overlies the Karalundi Formation and forms a predominant proportion of the succession in the Bryah Basin. It is composed of voluminous mafic to ultramafic volcanic rocks, and intrusive rocks. The mafic rocks contain pillow basalt, hyaloclastite basalt, sheeted dykes, a layered mafic-ultramafic igneous complex and minor felsic rocks, and show evidence for sea floor metasomatism in the form of tremolite-talc-chlorite-bearing assemblages (Pirajno and Occhipinti 2000; Pirajno et al. 2000; Occhipinti et al. 2004). The Narracoota Formation is overlain by metasediments of the Ravelstone Formation and Horseshoe Formation, which include wacke, shale, siltstone, chert and banded iron formation (Pirajno et al. 2000). Rocks of the Bryah Group have undergone multiple stages of deformation and greenschist facies metamorphism during formation of the Capricorn Orogen in the Proterozoic (Hynes and Gee 1986; Reddy and Occhipinti 2004).

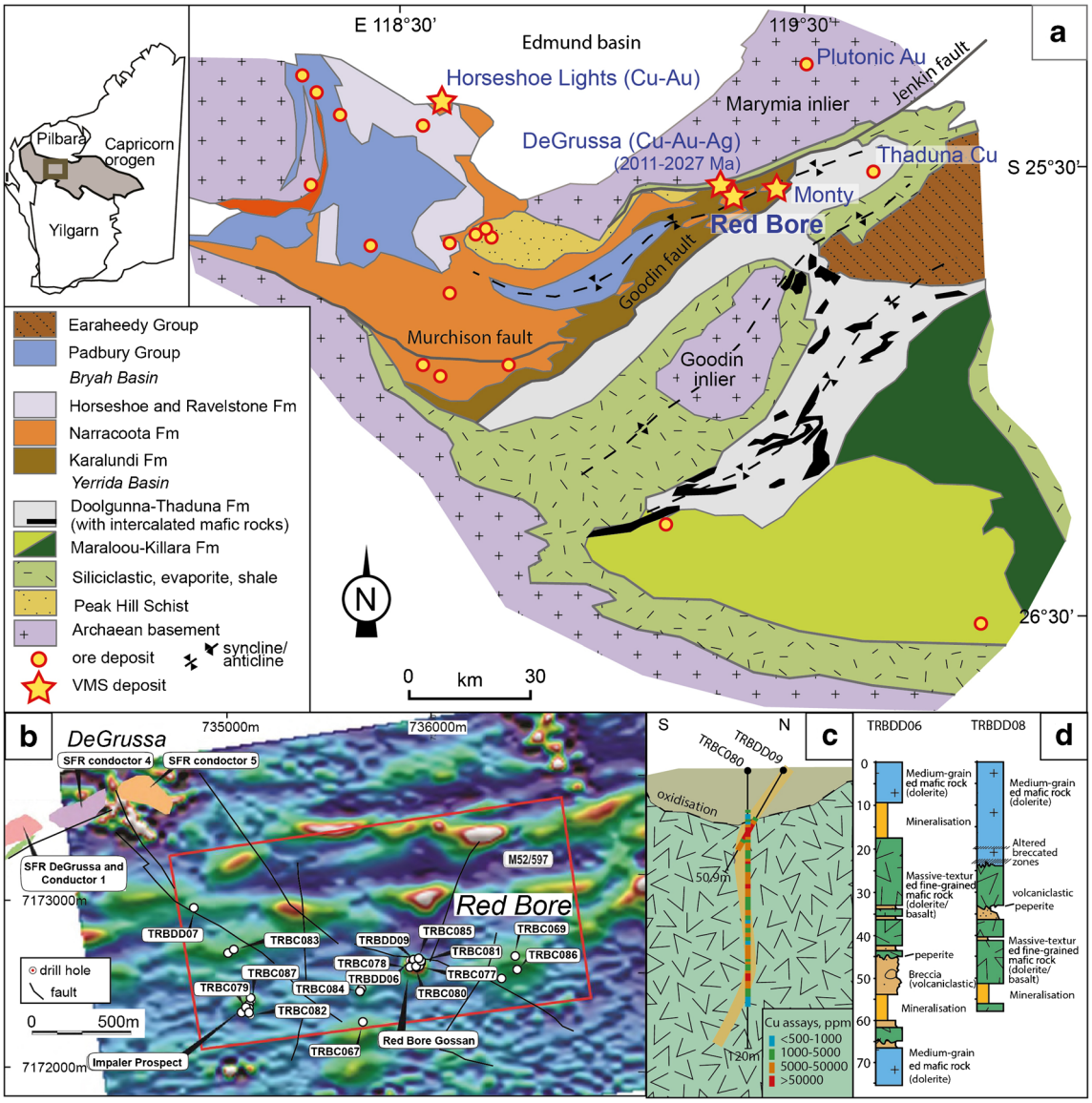

Fig. 1 **a** Simplified geological map of the Bryah, Padbury, and Yerrida Basins and distribution of VHMS and other ore deposits. Inset: location of the Capricorn Orogen in Western Australia between the Pilbara and Yilgarn cratons is indicated in grey shade. Modified from Pirajno et al. (2000); sulphide Re-Os ages from Hawke et al. (2015b). **b** Map of magnetic anomalies of the Red Bore area with location of some drill holes. Airborne magnetic survey included 1799 km flown at sensor height of 30 m using a Radiation Solutions RD-500 spectrometer (more information on the magnetic survey available in the 09/02/2015 Report at www.thundelarra.com/news/). **c** Down-hole plots of Cu assays. **d** Simplified logs of two cores (TRBDD06 and TRBDD08)

Sediments and mafic rocks associated with the Karalundi and Narracoota formations contain Cu-Au-Ag VHMS deposits at DeGrussa and Horseshoe Lights and the high-grade Monty deposit (Pirajno et al. 2000; Hawke et al. 2015b; Sandfire Resources Report, 2016). The Cu-Au-Ag DeGrussa deposit is mostly hosted in turbiditic sedimentary rocks, and consists of four steeply dipping lensoid ore lodes separated from each other by two large faults, with a combined strike length of 800 m. Due to deformation related to the Jenkin fault (Fig. 1) and the lack of outcrop, the stratigraphic relationships between DeGrussa and Red Bore are not clear in the field. The stratabound sulphides at DeGrussa are massive, fine-grained and consist of pyrite, chalcopyrite, and pyrrhotite with lesser sphalerite, galena, marcasite, and molybdenite. Chalcocite, malachite, azurite, chrysocolla, cuprite and native copper are present in the supergene ore zone. VHMS mineralisation at DeGrussa has recently been dated at 2027–2011 Ma (Re-Os on molybdenite) and 2040–2030 Ma (Pb-Pb on galena modelled according to Stacey and Kramers 1975), an age overlapping with the age of volcanism (Hawke et al. 2015b). Total estimated resources at April 2016 are 10.7 Mt. of ore containing 4.5% Cu and 1.8 g/t Au (Sandfire Resources Report 2016). The Monty deposit is composed of

chalcopyrite, pyrite and pyrrhotite with minor sphalerite and galena, and contains resources of 700,000 t at approximately 10% Cu and 2 g/t Au (Sandfire Resources Report 2016).

Drill core description

Surface expression of Red Bore mineralisation is represented by the presence of a gossan and a geographically restricted magnetic anomaly (Fig. 1b). Closely spaced drilling (more than30 drill holes, a few m to a few tens of m apart) carried out by Thundelarra Ltd. has intersected steeply-dipping elongate mineralisation containing massive chalcopyrite and massive magnetite. The mineralisation does not extend along strike, suggesting a "pipe-like", rather than tabular geometry. Double intersections may indicate the presence of two separate mineralised bodies or tectonic duplication. Drill core lithology is dominated by dolerite, coarse (mm-scale)-grained massive mafic rocks (gabbro, ultramafic rocks), mafic volcanic and volcaniclastic rocks (lava and possibly hyaloclastite), and fine-grained, finely-bedded sedimentary rocks. Mineralisation is largely hosted in mafic rocks (mostly dolerite) of the Narracoota Formation and to a lesser extent, by sedimentary rocks. The mineralisation extends from the near-surface (shallowest intersection at 6 m depth) to at least ~ 100 m (Fig. 1c). The mineralisation is open at depth, and its total extent is not known.

In several samples, the volcanic-intrusive host rocks show signs of semi-brittle deformation. The mineralisation is surrounded by a narrow (< 2 m wide) alteration zone represented in core samples by a fine-grained "bleached" pale green rock mostly composed of talc, carbonate, chlorite and silica. There is no evidence of a hydrothermal system (veins) developed around the mineralisation, as veins were not intersected outside the mineralised zone.

Analytical techniques

Samples collected during this study were analysed using scanning electron microscopy, whole- rock geochemistry, laser-ablation inductively coupled plasma mass spectrometry, secondary ion mass spectrometry for multiple S isotopes and negative thermal ionisation mass spectrometry for Re-Os isotopes. Analytical methods are presented in ESM E-1.

Sample description

Drill core description

The cores have intersected mineralisation for a length of up to 10–12 m and show a zoned distribution of minerals, with a massive chalcopyrite zone (up to 7 m) in the centre and a discontinuous massive magnetite zone at the margin (see ESM E-2 for drill hole locations and orientation). The central ore zone (Fig. 2a) is composed of massive chalcopyrite (> 90%; for example, a 7.05-m intersection at 28.4 wt% Cu, 1.3 ppm Au and 32 ppm Ag was found in drill core TRBDD09) with needle-like silicate inclusions, pyrite and minor covellite [CuS]. The marginal zone is composed of massive magnetite (> 90%) with minor chalcopyrite and pyrite, and carbonate-rich veinlets (Fig. 2b). The mineralisation is oxidised in the top 25 m, and contains Fe- and Cu-oxy-hydroxides. In addition, disseminated pyrite and chalcopyrite are hosted by finely-bedded sedimentary rocks in the south-western part of the tenement.

The massive magnetite is brecciated in places, forming a monomictic matrix-supported chaotic breccia (Fig. 2b). Clasts of this breccia are mostly angular, up to ~ 10 cm in size, composed of magnetite-replaced mafic rocks, and are cross-cut by brown carbonate veinlets. These veinlets do not cross-cut the surrounding matrix. The matrix has a grain size of up to a few mm and is composed of magnetite and silicate minerals. Cement between clasts could not be identified from hand specimens. Minor sulphide veinlets (chalcopyrite in particular) cross-cut both the matrix and the clasts (Fig. 2c).

Microtextures

Massive chalcopyrite ore contains abundant elongate silicate inclusions, such as amphibole and talc, which have been variably silicified (Fig. 3a). These silicate inclusions are distributed along planes, thus defining a foliation, although individual crystals are randomly oriented, and are interpreted as hydrothermal. Sulfidation of silicate needles can be observed in some cases, whereby chalcopyrite or pyrite form μm-scale grains on previous silicates (Fig. 3b). Samples of massive magnetite are non-foliated and composed of sub-round magnetite grains, up to 100 μm in size, which are partly rimmed by haematite. Massive magnetite samples contain chalcopyrite and pyrite occurring as mm- to sub-mm-scale veinlets or as interstitial grains (Fig. 3c). In addition, magnetite is cross-cut by Fe-carbonate veinlets that also contain Ca-amphibole and minor sulphide phases (chalcopyrite, sphalerite, Co-sulphide) (Fig. 3d). Semi-quantitative EDS analyses indicate that sphalerite contains up to 7.5 wt% Fe.

Pyrite occurs in both massive chalcopyrite and massive magnetite samples as anhedral grains and veinlets with an apparent "cleaved" texture (Fig. 3b). EDS semi-quantitative analyses indicate the presence of variable amounts of Co and high-magnification SEM images suggest a nanoscale granular texture. This pyrite may by the product of sulfidation of a silicate (e.g. amphibole). Bismuth-Te-Se phases, in some

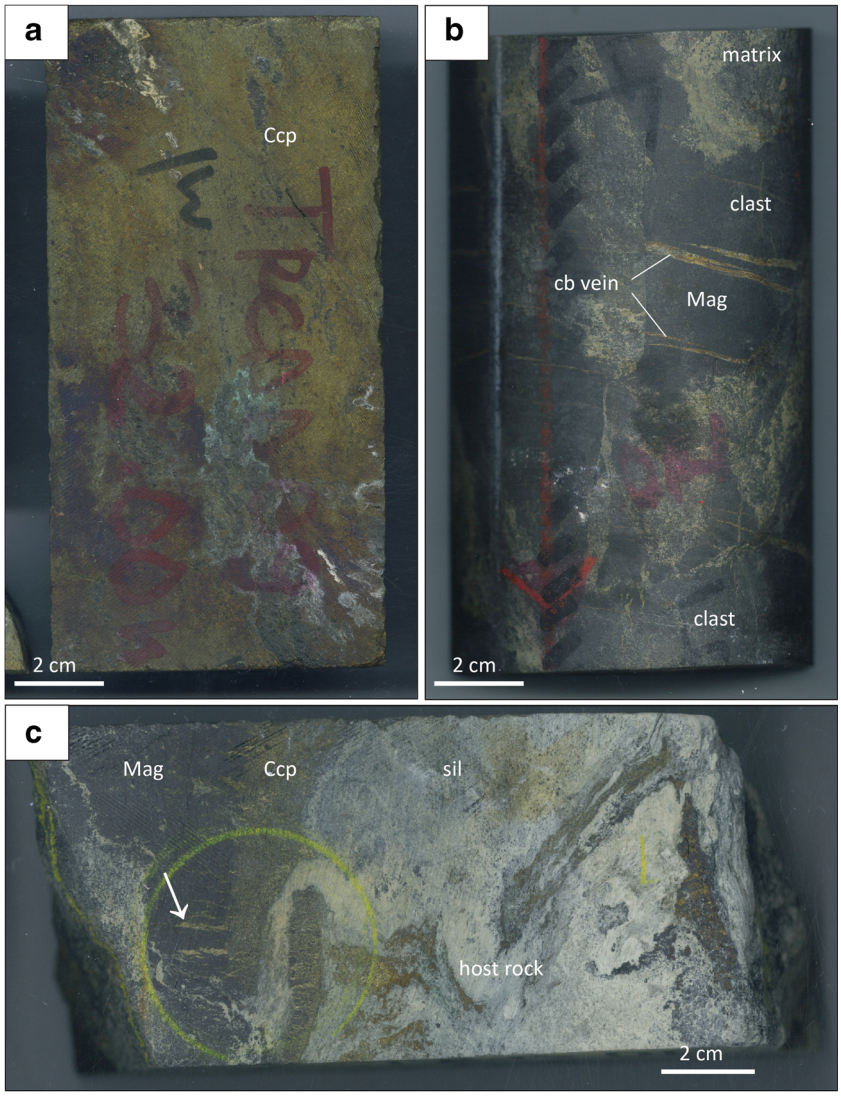

Fig. 2 Drill core samples from Red Bore. **a** Massive chalcopyrite, sample TRCDD09 32.0 m. **b** Massive magnetite breccia. Clasts are cross-cut by Fe-Ca-carbonate (cb) veinlets that do not extend into the matrix. **c** External contact of the ore body. Chalcopyrite veinlets (Ccp, some arrowed) truncate magnetite (Mag) at the contact with talc-silica-carbonate-amphibole altered host rock (sil)

cases coexisting with a Te-Ag phase (Fig. 3b–e), occur either as inclusions up to 50–60 μm in size or along μm-scale veinlets in pyrite and chalcopyrite. These Bi-Te-Se grains contain between ~24–41 wt% Te, and ~5 and 10 wt% Se (EDS). Anhedral S-Co-O-Si grains that show zoned texture in BSE images occur in both massive chalcopyrite and massive magnetite samples. X-ray element maps of these grains indicate that S, Cu and Co (up to 35 wt%) are enriched at the margins and along cracks, whereas Si and O contents decrease towards grain margins and cracks (Fig. 3f), thus indicating replacement of a silicate mineral. Copper sulphide (~$CuS_{0.9}$ covellite, of likely supergene origin) occurs as anhedral, cracked grains in massive chalcopyrite. The alteration halo around mineralisation contains Mg-Fe silicate (Fe-bearing talc, or minnesotaite), Si, Ca-Fe-carbonate, Ca-(±K)-bearing amphibole and chlorite. Semi-quantitative EDS analyses indicate that this amphibole contains 11–21 wt% CaO and Mg/(Mg + Fe) = 0.41–0.71.

Analytical results

Bulk assays

Bulk assays indicate contents of Cu from 0.03 to 30.1 wt%, Au up to 20 ppm and Ag up to 40 ppm (Fig. 4). Copper concentrations have a broad positive correlation with Au and Ag, although some analyses have distinctively high Au and Ag and relatively low Cu (Au/Cu × 10,000 ≥ 5). There is also a broad negative correlation between Au/Cu and Ag, indicating that the highest Au/Cu values are found in moderately chalcopyrite-rich samples.

Mineral chemistry (LA-ICP-MS)

Chalcopyrite contains up to ~8 ppm Au and up to 240 ppm Ag (Fig. 5, ESM Table 1). The highest Au and Ag concentrations were measured in chalcopyrite veinlets emplaced at the

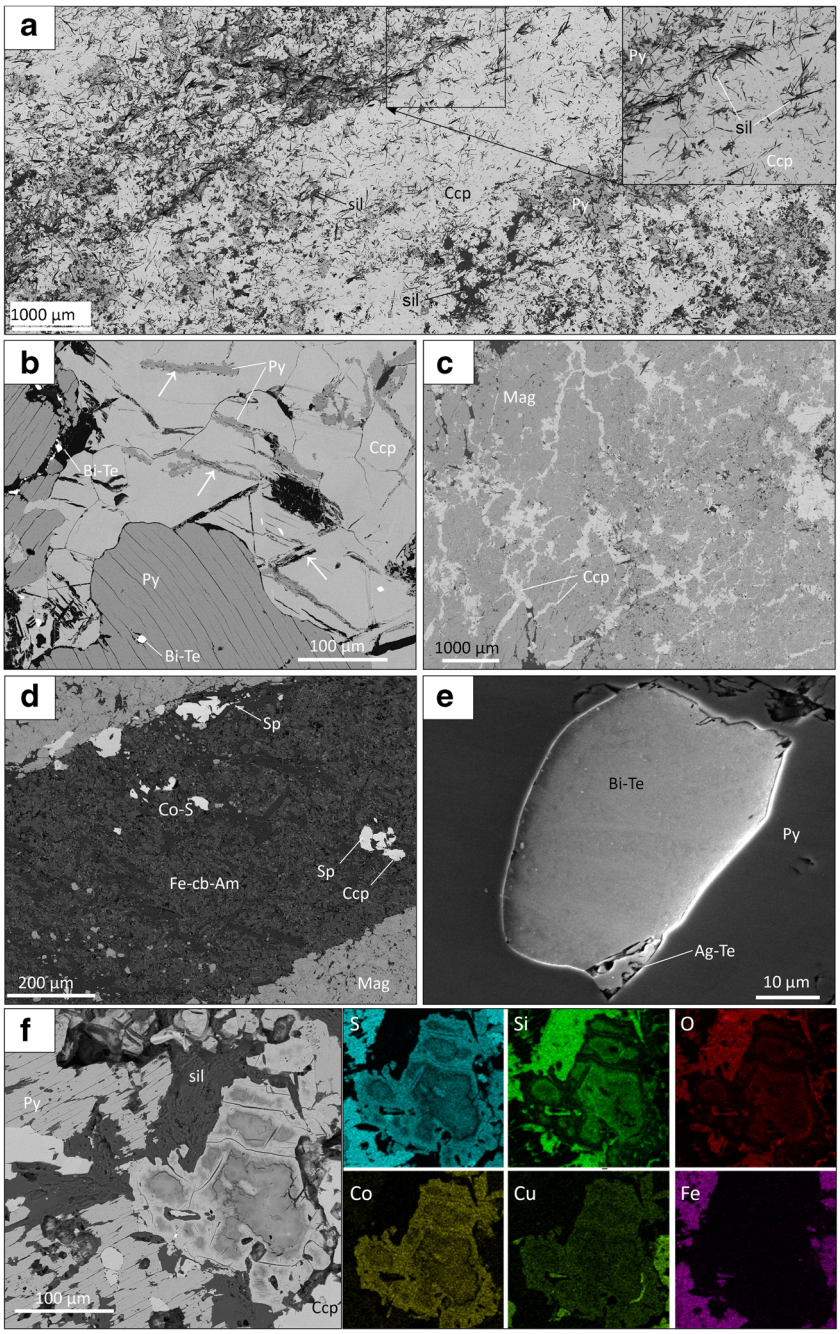

Fig. 3 Ore microtextures at Red Bore. **a** (and inset) Massive chalcopyrite with needle-like silicate inclusions. BSE image, sample TRBDD09 35.5 m. **b** Anhedral pyrite and partially sulfidised silicate needles (some arrowed) in chalcopyrite. Note the "cleaved" texture of pyrite. BSE image, sample TRCDD09 31.5 m. **c** Massive magnetite with chalcopyrite veinlets. BSE image, sample TRCDD04 31.5 m. **d** Fe-carbonate-amphibole veinlet with minor sulphides (chalcopyrite, sphalerite, Co-sulphide) cross-cutting massive magnetite. BSE image, sample TRBDD09 38 m. **e** Inclusion of Bi-Te and Ag-Te in pyrite. BSE image, sample TRCDD04 31.5 m. **f** BSE image and X-ray element maps of zoned S-Co-O-Si mixed phase in strongly silicified needle-like crystals (BSE, sample TRBDD09 35.5 m). Note S-replacement along rim and cracks (sulfidation of silicates). Abbreviations: Am amphibole, cb carbonate, Ccp chalcopyrite, Mag magnetite, Py pyrite, Sp sphalerite, sil silicates (variably silicified talc and amphibole)

margin of the mineralised body (sample TRBDD08 51.7 m). Tellurium is mostly < 10 ppm and Bi < 30 ppm in both chalcopyrite and pyrite, although the presence of Bi-Te ± Se inclusions resulted in significantly higher concentrations (Bi and Te up to more than 1000 ppm) and positive correlations between these elements in some spot analyses. Selenium content (mostly ~ 100–1200 ppm in chalcopyrite) is strongly variable between samples but has narrow ranges within samples and between minerals of the same samples (Fig. 5). Plots of signal intensity as counts per second (cps) versus analysis time (s) confirm the presence of various inclusions of Bi-Te ± Se and Te ± Ag ± Au phases in both chalcopyrite and pyrite (Fig. 6). Selenium concentrations are only partly controlled by inclusions.

Chalcopyrite contains higher Zn and Sn concentrations (~ 10 to 740 ppm Zn) than other minerals (pyrite contains < 50 ppm Zn). Molybdenum concentrations of chalcopyrite at the margin of the ore body (TRDCC09 35.5 m) are higher and more variable (Mo ~ 1–80 ppm) than those from the centre (Fig. 5). Pyrite is the main carrier of Ag (~ 300–600 ppm), Pb (~ 30–700 ppm), Tl (~ 1–15 ppm), Cr and Re (up to ~ 3 and 1.4 ppm, respectively), and has low concentrations of As and

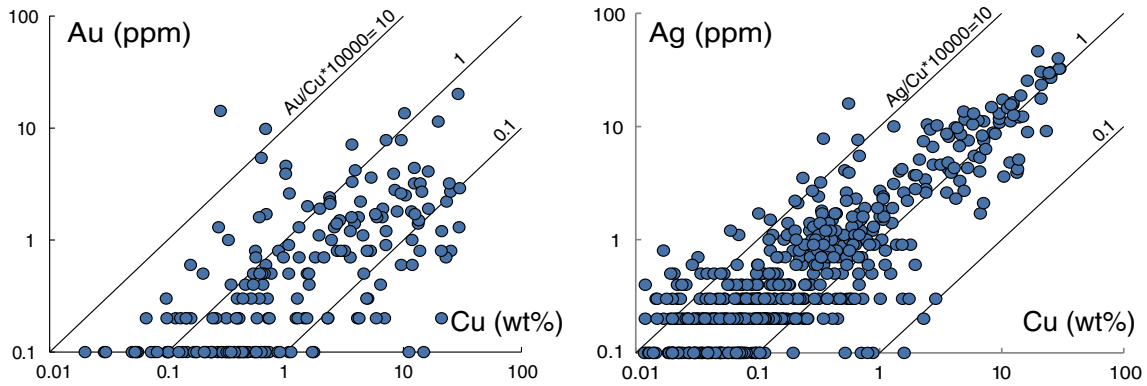

Fig. 4 Bulk rock assays of Red Bore samples (ICP-OES and ICP-MS). Au and Ag as ppm, Cu as wt%

Sb (< 20 ppm and < 1 ppm, respectively). Magnetite has low concentrations of Ti (< 70 ppm), V (< 60 ppm) and Ni (up to 30 ppm) and overlaps with magnetite from banded iron formation and metamorphic magnetite in the discrimination plots of (Nadoll et al. 2014) (Fig. 7). However, manganese (up to 2500 ppm Mn) is higher than hydrothermal magnetite, and similar to magmatic magnetite from mafic rocks (Dare et al. 2014). The Cu content of magnetite is between 50 and 2600 ppm (omitting a few higher outlying values likely due to chalcopyrite inclusions), and Sn is between 1 and 10 ppm.

Values of $^{208}Pb/^{206}Pb$ and $^{207}Pb/^{206}Pb$ of chalcopyrite and pyrite measured by LA-ICP-MS during trace element analysis span a wide range ($^{208}Pb/^{206}Pb$ ~ 0.48–2.30), and define a linear trend in the $^{208}Pb/^{206}Pb$ vs. $^{207}Pb/^{206}Pb$ plot (ESM Fig. 1). The highest values of $^{208}Pb/^{206}Pb$ and $^{207}Pb/^{206}Pb$ overlap with values expected from Palaeoproterozoic crust according to the model of Stacey and Kramers (1975). Disseminated chalcopyrite and pyrite largely overlap with $^{208}Pb/^{206}Pb$ and $^{207}Pb/^{206}Pb$ measured at DeGrussa (Hawke et al. 2015b; Belousov et al. 2016). Overall the values define a rather continuous trend, but spot analyses of sulphides forming veinlets in massive magnetite samples have more radiogenic (lower) values of $^{208}Pb/^{206}Pb$ and $^{207}Pb/^{206}Pb$ in comparison with analyses from massive and, especially, disseminated mineralisation.

In situ S isotope analyses (SIMS)

Multiple S isotopes (^{32}S, ^{33}S and ^{34}S) of chalcopyrite and pyrite were analysed in eight samples collected at down-hole depths between 31.5 and 66.0 m from five cores. Chalcopyrite and pyrite yielded $\delta^{34}S$ between + 1.12 and + 4.63‰, and $\delta^{34}S$ values between − 0.27 and + 4.19‰, respectively (Fig. 8, ESM Table 2). However, most analyses of both pyrite and chalcopyrite (> 80% of the 87 spots) yielded $\delta^{34}S$ values between + 3.0 and + 4.6‰ (Fig. 8). Values of $\delta^{34}S$ below + 3.0‰ are mostly scattered, and lie up to 2‰ lower than other analyses in the same sample (Fig. 8b). If these outlying analyses are excluded, ranges of $\delta^{34}S$ in single samples are extremely narrow (≤ 1‰). Variations of $\delta^{34}S$ between samples do not correlate with sampling depth or sample texture (i.e. massive or veinlets). In samples where both phases were analysed, chalcopyrite tends to have slightly higher $\delta^{34}S$ values than pyrite (~ 0.5–0.8‰ on average, greater than the $\delta^{34}S$ 2σ error of 0.33‰ for chalcopyrite). Deviations from mass-dependent fractionation are not significant ($-0.1 < \Delta^{33}S < +0.05$‰).

Re-Os isotope analyses

The samples have Re and Os contents of 6.20–99.6 ppb and 59.5–1030 ppt, respectively. $^{187}Re^{188}/Os$ ratios are between 1770 and 57,900, and have a broad positive correlation with $^{187}Os/^{188}Os$ ratios. The regression on all ten analyses gives a very poor age of 1030 ± 170 Ma (MSWD of 9050) and a meaningless negative initial $^{187}Os/^{188}Os$ of − 45. A regression on six out of ten analyses (excluding samples BM002185 and BM002188) yielded a marginally improved age of 959 ± 110 Ma (MSWD of 50), and an initial $^{187}Os/^{188}Os$ of 40 (ESM Fig. 2).

Discussion

Sulphide deposition from a magmatic fluid at Red Bore? Geologic, elemental and isotopic evidence

In VHMS deposits, elemental and isotopic data of the ore and associated alteration have been used to support either derivation of metals from sea water leaching of surrounding rocks or derivation from magmas. However, these data can be equivocal as "magmatic" signatures may be acquired either by direct magmatic-hydrothermal input or by leaching of volcanic rocks by circulating sea water (Huston et al. 2011; Urabe

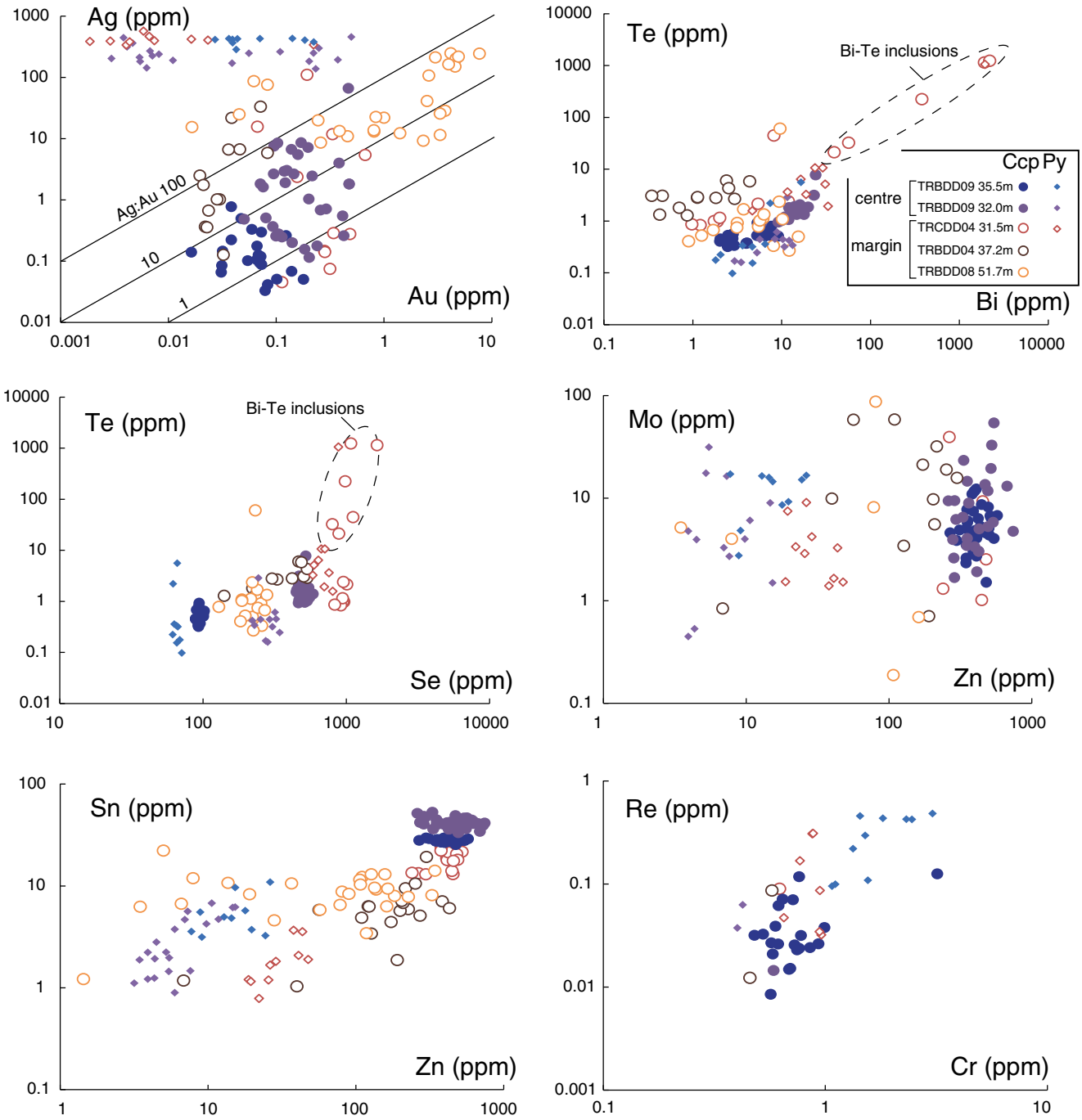

Fig. 5 Trace element composition of chalcopyrite and pyrite from Red Bore (LA-ICP-MS, all compositions as ppm). Samples from the centre (massive chalcopyrite) and the margin (massive magnetite) of the mineralised body are distinguished

and Marumo 1991). Therefore, the role of magmatic fluids in the formation of VHMS mineralisation can be better evaluated based on a combination of factors, including deposit- to micro-scale geological and textural observations, mineral associations and geochemical data. For example, in VHMS systems associated with felsic magmatism, the spatial association of VHMS mineralisation with intrusions (Galley 2003) and with aluminous, advanced argillic alteration, similar to alteration typically associated with porphyry style deposits (e.g. at Mt. Lyell; Large et al. 1996) has been used to infer a causative relationship between granitic magmatism and mineralisation. In contrast to these felsic-associated systems, talc-carbonate-silica-amphibole alteration assemblages at Red Bore resemble those found in mafic-hosted sea floor hydrothermal systems. In mafic volcanic-hosted VHMS deposits of Cyprus, typical alteration assemblages are

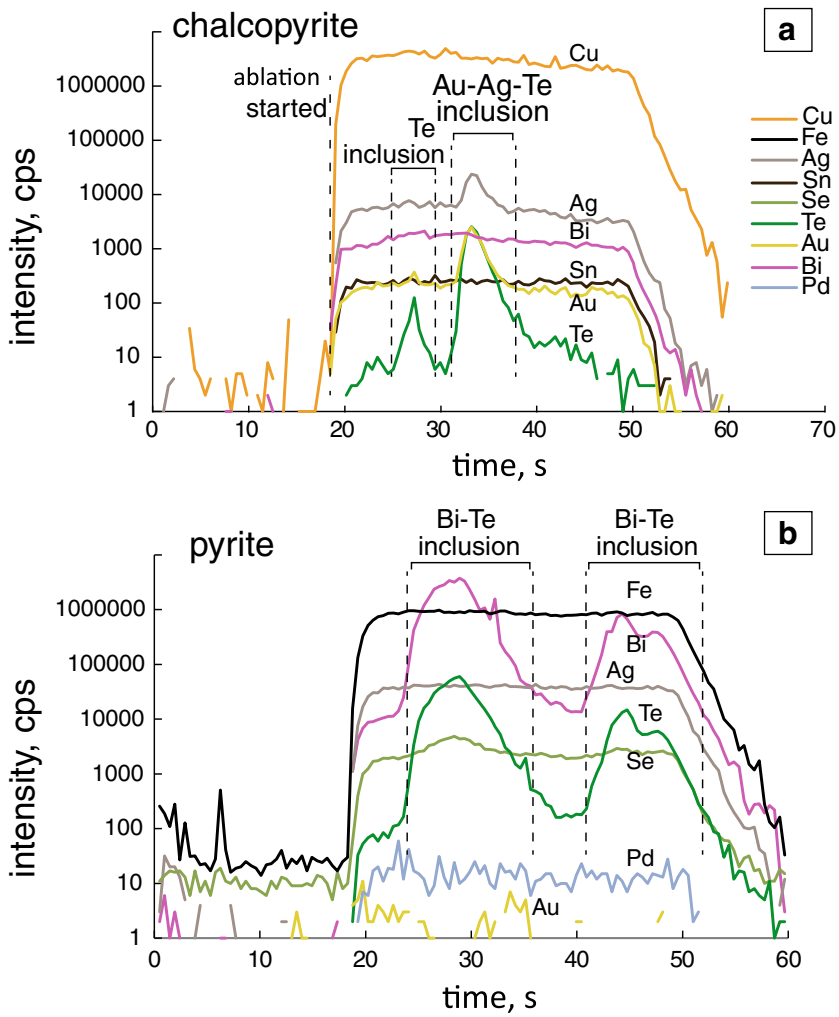

Fig. 6 Laser ablation signal as counts per second (cps) of chalcopyrite (**a**) and pyrite (**b**) plotted versus analysis time (s). Co-occurrence of element peaks indicates the presence of Te-Au-Ag and Bi-Te inclusions. **a** Total Au = 7.7 ppm, sample TRBDD08 51.7 m. **b** Total Au = 0.02 ppm, sample TRCDD09 31.5 m

dominated by quartz and chlorite, replacement of feldspar, with local epidote and haematitic jasper (Adamides 2010). These deposits show evidence of deposition both at the surface (exhalative) and in the subsurface. Most deposits occur along faults, and mineralisation textures indicate replacement of host rocks (Adamides 2010). At Rudny-Altai, where Besshi-style deposits hosted in mafic igneous and sedimentary rocks have been recognised, the alteration assemblage is dominated by amphibole (anthophyllite), chlorite and quartz (Lobanov et al. 2014).

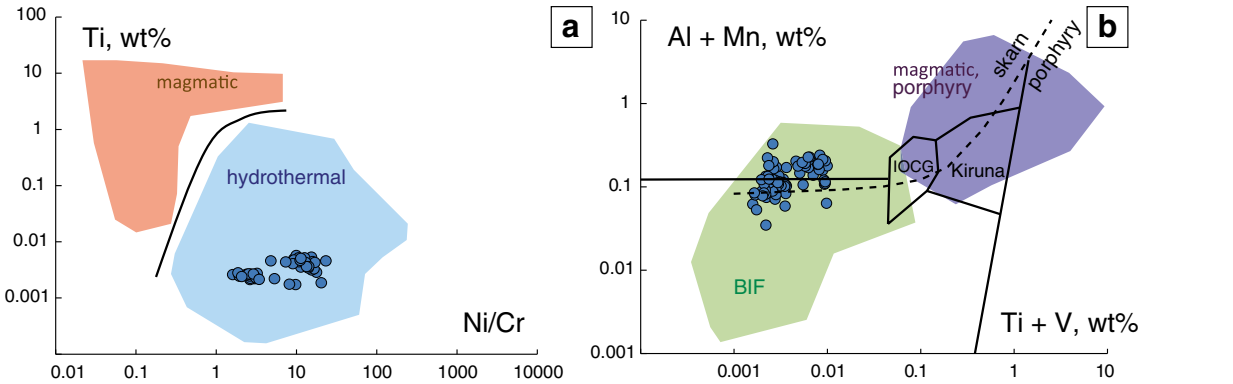

Fig. 7 Trace element compositions of magnetite at Red Bore (LA-ICP-MS). **a** Ti vs Ni/Cr diagram; line distinguishing magmatic and hydrothermal magnetite and fields from Dare et al. (2014). **b** Al + Mn vs. Ti + Mn (wt%) diagram from Dupuis and Beaudoin (2011), BIF field modified according to Nadoll et al. (2014)

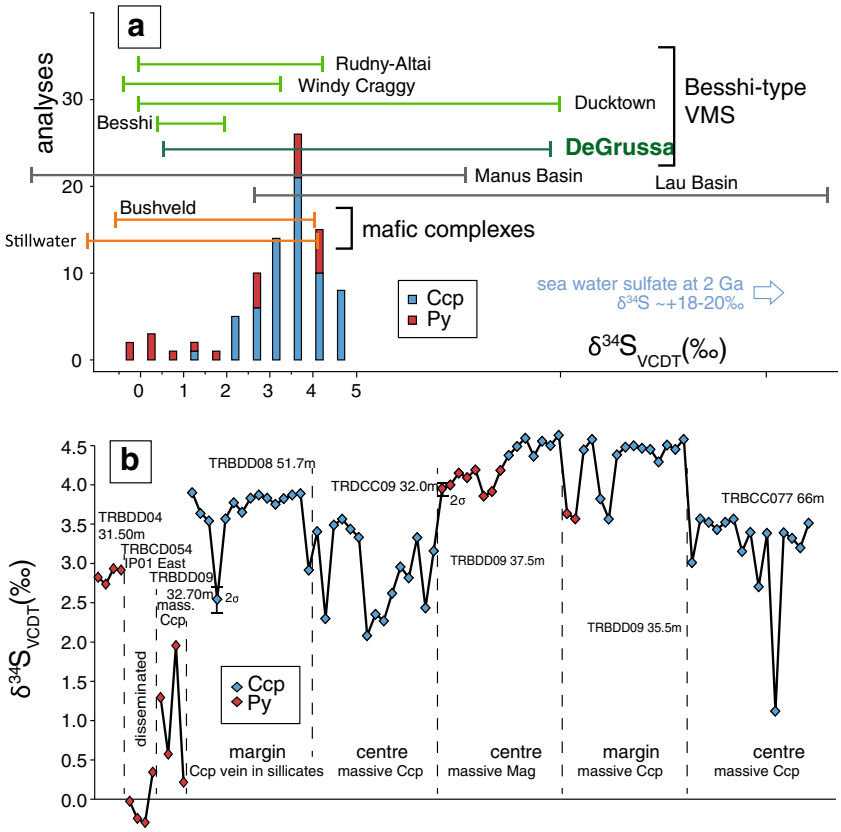

Fig. 8 Sulphur isotope compositions at Red Bore (SIMS). **a** Histogram. **b** Plots of single analyses distinguished by sample and mineral phase. Abbreviations: Ccp chalcopyrite, Py pyrite. Ranges of $\delta^{34}S$ for VHMS deposits (DeGrussa; Hawke et al. 2015a; Bell 2016; other data compiled by Lobanov et al. 2014) and S-poor mafic complexes are shown for comparison; Bushveld and Stillwater complexes (from Ripley and Li 2003)

The enrichment in Cu, Au and Ag is typical of VHMS deposits associated with mafic volcanic rocks, either Cyprus/Besshi-types (Galley et al. 2007; Adamides 2010), or mid-oceanic ridge style (Murphy and Meyer 1998). High concentrations of these elements may indicate a magmatic association even in other types of VHMS deposits. For example, after reviewing radiogenic and stable isotope data on Kuroko-type deposits, Urabe and Marumo (1991) concluded that most Cu is of magmatic origin. In contrast, Ohmoto (1996) attributed most metals to leaching of host lithologies by circulating sea water derived fluids. The tendency of Cu and other chalcophile elements, such as Au and Ag, to partition into magmatic fluids coexisting with silicate melts is well-reported (Lowenstern et al. 1991; Heinrich et al. 1992). For example, in mafic magmas of the Manus basin, a sudden decrease of Cu and Au during fractionation has been interpreted as evidence of loss of these elements to an exsolving S-rich volatile phase (Sun et al. 2004). Magmatic vapours derived from mafic magmas tend to be Cu-rich and Cu-phases such as chalcocite (Cu_2S), covellite (CuS) and chalcopyrite have been found as incrustations formed by these fluids at volcanic vents or trapped as fluid inclusions in phenocrysts (Simon and Ripley 2011; Agangi and Reddy 2016). In modern submarine hydrothermal systems, several studies suggest that magmatic volatiles are likely responsible for the transport and deposition of metals such as Cu and Au and other chalcophile elements (de Ronde et al. 2005, 2014; Berkenbosch et al. 2012; Petersen et al. 2014). High Se contents in VHMS deposits are also considered as indicative of derivation from a magmatic source (Hannington 2014), although others have proposed that Se could be sourced from black shales (Layton-Matthews et al. 2008). Selenium concentrations in pyrite and chalcopyrite at Red Bore and at DeGrussa are high in comparison with other VHMS deposits in Western Australia (Belousov et al. 2016), which may provide further indications of a magmatic input. Similar high Se values have been measured in bulk samples of ultramafic-hosted VHMS (Murphy and Meyer 1998) and in single sulphide phases from mafic-ultramafic modern VHMS deposits (Wohlgemuth-Ueberwasser et al. 2015) (Fig. 9).

Bi-Te-(Se) phases have only in some cases been described in VHMS deposits, as occurring in the deep portion of deposits (Cu-rich stringer zone) in the Iberian Pyrite Belt (Marcoux et al. 1996) and Jabal Sayid deposit of Saudi Arabia (Sabir 1980) or in sulphide chimneys (Maslennikov et al. 2013; Berkenbosch et al. 2012). Besides VHMS deposits, Bi-Te phases have been reported in orthomagmatic, skarn, porphyry and epithermal deposits, where they form compounds with Au, Ag, Pt group elements and other precious metals (Ciobanu et al. 2005, 2006; Dora et al. 2014). Te-

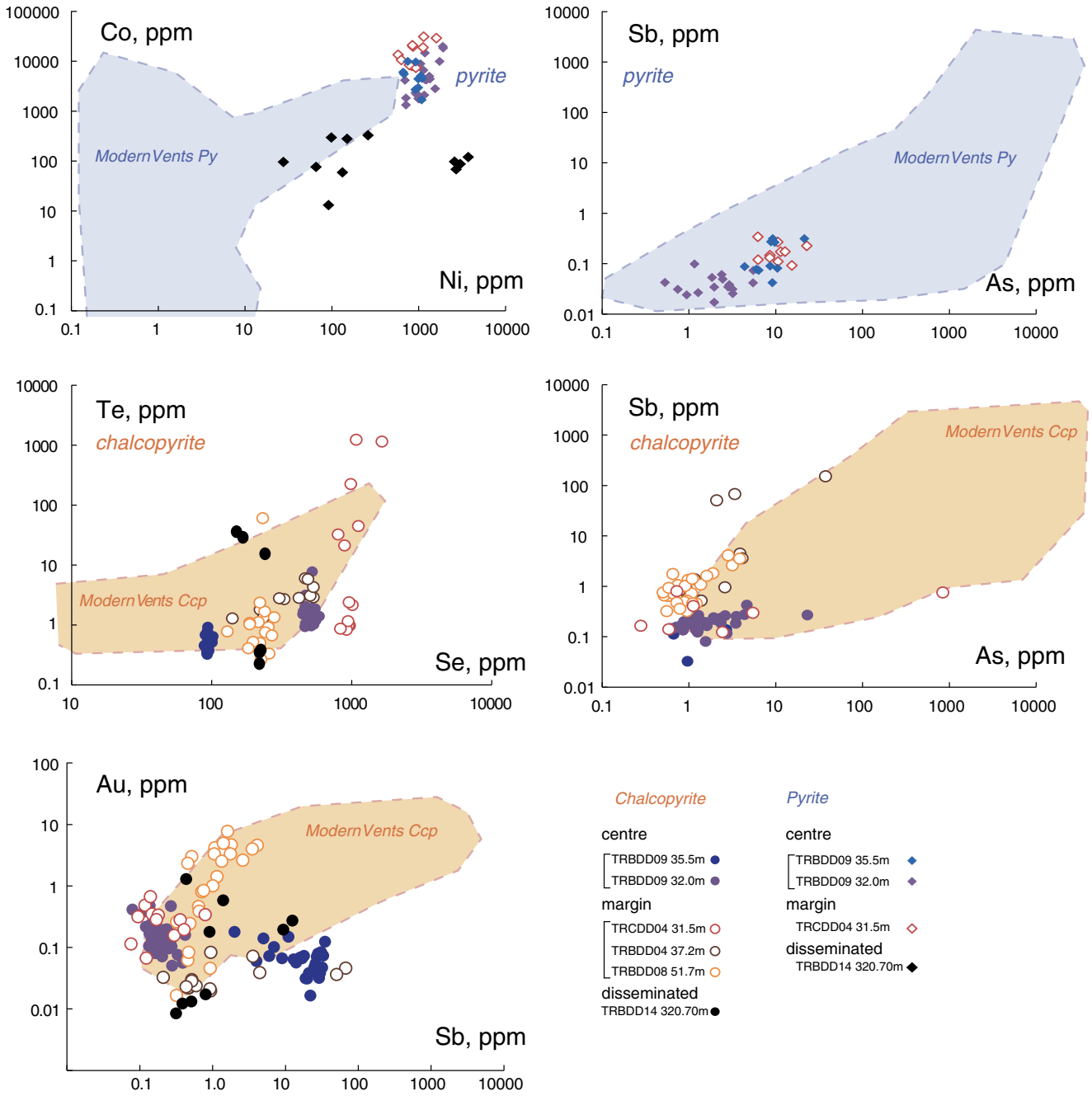

Fig. 9 Composition of pyrite and chalcopyrite from Red Bore (LA-ICP-MS, all compositions as ppm), including disseminated mineralisation compared with pyrite from modern submarine vents formed in a comparable spreading setting (Wohlgemuth-Ueberwasser et al. 2015; Keith et al. 2016)

Bi-(Au) phases are also known to be deposited from high-temperature volcanic gases (Symonds et al. 1987; Henley et al. 2012), and Te intake in chalcopyrite is believed to be enhanced at high temperature (Hannington et al. 1991). Therefore, Te, Bi, Se and Au, as a suite are compatible with a magmatic-hydrothermal derivation and have been proposed as being indicative of a magmatic source (Galley et al. 2007; Berkenbosch et al. 2012; Lehmann et al., 2013).

Values of $\delta^{34}S$ in VHMS deposits overall span a wide range (Hannington 2014; Lobanov et al. 2014). The fact that many VHMS deposits contain sulphates with $\delta^{34}S$ that mirrors the $\delta^{34}S$ of sea water at the time of deposition is good evidence for direct involvement of sea water sulphate (Huston et al. 2010). However, VHMS hosted in mafic-dominated volcano-sedimentary successions tend to have narrow ranges of $\delta^{34}S$ (Besshi-type ~0–4‰, Fig. 8) in comparison with felsic volcanic-hosted VHMS deposits,

which have higher and more varied S isotope compositions (Lydon 1984; Petersen et al. 2014; Hannington 2014; Cloutier et al. 2015). Vent fluids discharged at sediment-poor mid-ocean ridges also tend to have narrow $\delta^{34}S$ ranges (between 0 and 6‰; Marini et al. 2011). In sulphide-poor mafic complexes, such as the Merensky Reef of the Bushveld Complex or the Stillwater Complex, for which the S may have been accommodated by the melt, rather than incorporated from country rocks, sulphides have similar compositions, $\delta^{34}S = 0–4‰$ (Ripley and Li 2003) (Fig. 8). The homogeneity of most $\delta^{34}S$ values (80% of analyses are between + 3.0 to + 4.6‰, Fig. 8) of chalcopyrite and pyrite at Red Bore is consistent with precipitation from a homogenous (one-phase) fluid of magmatic origin. Precipitation of chalcopyrite from H_2S is expected to cause relatively minor fractionation of S isotopes ($\delta^{34}S$ variation < 1 ‰; Kajiwara and Krouse 1971). Thermochemical sulphate reduction results in strong fractionation between sulphate and sulphide ($\delta^{34}S$ sulphate - $\delta^{34}S$ sulphide = 17‰ at temperatures of 300–350 °C, relevant for Red Bore; Ohmoto 1986). Assuming a Palaeoproterozoic sea water sulphate $\delta^{34}S$ value of ~ 20‰ (Farquhar et al. 2011, ESM Fig. 3), sulphide originated through this mechanism would have $\delta^{34}S = 3–20$ ‰, depending on the proportion of sulphate reduced. However, the fact that no sulphate was found at Red Bore may indicate that the fluids were relatively reduced and sulphate was not the dominant species in the mineralising fluids (Murphy and Meyer 1998). Biogenic sulphate reduction produces sulphide with strongly negative $\delta^{34}S$ (≥−30‰). Thus, the absence of $\delta^{34}S < 0‰$ in our samples is not compatible with such processes. Further, the absence of mass-independent fractionation of S isotopes excludes the possibility that sedimentary S may have been remobilised from surrounding Archaean terrains (Bekker et al. 2009).

The slightly lower and scattered $\delta^{34}S$ measured in some of our analyses ($\delta^{34}S \sim < 2.5‰$) may be due to minor events of phase separation in the mineralising fluid. Vapour separation is associated with partial oxidation of S to form SO_4^{-2} (Drummond and Ohmoto 1985) according to the equation $H_2S\ (aq) + 4H_2O \rightarrow SO_4^{2-}(aq) + 2H^+ + 4H_2(g)$. Separation of a SO_4^{2-}-rich vapour would have preferentially extracted heavy S isotopes, imparting lower $\delta^{34}S$ values to the remaining fluid. This may have occurred locally during transient pressure release due to, for instance, tectonic movements. However, later remobilisation processes related with the long and complex tectonic history of the basin cannot be excluded.

Secondary remobilisation revealed by Re-Os and Pb-Pb isotopes

Given the scatter of Re-Os isotope values, we do not attribute any specific geochronological meaning to these analyses. The Re-Os data indicate Re and Os remobilisation during the complex tectonic history of the area. The linear trend observed in plots of Pb isotope ratios can be explained as due to two end-member mixing of crustal Palaeoproterozoic Pb and a highly radiogenic Pb component. The age of this Pb mixing event cannot be constrained, and it is not clear whether the two events indicated by Re-Os and Pb systematics coincide. Thus, despite the fact that the textures, S isotopes and geochemical characteristics observed at Red Bore do not show obvious evidence of metamorphism or intense deformation, the occurrence of cryptic secondary remobilisation can be revealed by Re-Os and Pb isotope systems.

Red Bore and DeGrussa: part of the same hydrothermal system?

A genetic relationship between the Red Bore mineralisation and the strata-bound VHMS deposit at DeGrussa has been previously suggested (Hawke et al. 2015b; Pirajno et al. 2016). This interpretation is supported by the close spatial association, by mineralogical and geochemical arguments, for example the abundance of chalcopyrite, the enrichment in Cu, Au, Ag. However, the elongate geometry, level of mineralisation/grade (massive chalcopyrite with up to ~ 30 wt% Cu and low concentrations of Pb and Zn), the abundant massive magnetite mineralisation and the direct association with mafic intrusive host (dolerite) at Red Bore strongly contrast with DeGrussa and other VHMS deposits known in the region, which are mostly hosted by terrigenous sedimentary rocks. Typically, VHMS mineralisation tends to form sulphide-rich lensoid bodies, largely strata-bound and with thicknesses in the order of tens of metres and typically low aspect ratios (depth-to-lateral extent ratio). Massive sulphide mineralisation is formed at, or close to, the water-sediment interface, and is underlain by silica-sulphide stockwork style mineralisation (Shanks III 2012; Ohmoto 1996). Typical VHMS deposits associated with mafic volcanism have high Cu/(Cu + Zn) with Cu rarely exceeding 5–6 wt%, even in Cu-rich deposits (Galley et al. 2007; Shanks III 2012; Lobanov et al. 2014). Au-bearing pyrite-chalcopyrite discordant “pipes” have been described at Mount Morgan and Reward deposits, Australia (Large 1992). The Reward deposit has been attributed to the class of VHMS deposits based on the presence of strata-bound massive Zn-Pb-Cu lenses, alteration styles and ore textures (Large 1992). Murphy and Meyer (1998) described Au-rich massive chalcopyrite mineralisation hosted in mafic and ultramafic rocks of the Logatchev hydrothermal field of the Mid-Atlantic ridge. In these deposits, sulphate (anhydrite) is rare, whereas it is abundant in associated Zn-rich deposits, a feature that Murphy and Meyer (1998) attribute to limited sea water

contribution in Cu-rich deposits. The depth of deposition of the Red Bore mineralisation in the context of a submarine hydrothermal system cannot be assessed with certainty, given the absence of pressure indicators. However, the absence of widespread alteration suggests that the ore bodies did not form within the wide alteration zone typically associated with VHMS deposits.

At DeGrussa, reported $\delta^{34}S$ of sulphides span the range + 0.25 to +9.82‰ (Hawke et al. 2015a), overlapping with our results at Red Bore, but also extending towards higher values. This may be due to mixing of magmatic fluids with sea water at, or near, the surface. In sea floor hydrothermal systems, as magmatic fluids rise towards the surface, they will inevitably mix with sea water-derived fluids, so that the resulting sulphide deposits will carry the geochemical features of both components. In some VHMS systems where a magmatic input has been inferred, the upwards widening of ranges of $\delta^{34}S$ in present-day hydrothermal vents (Petersen et al. 2014) as well as the upwards increase of $\Delta^{33}S$ (− 1.5 to + 1.2) in Archaean VHMS (Jamieson et al. 2013) suggests that VHMS-forming fluids become progressively sea water-enriched as they rise towards the surface. Seawater sulphate contributions to ancient VHMS deposits and present-day systems are estimated to vary from 3 to > 40% (de Ronde et al. 2014; Jamieson et al. 2013; Chen et al. 2015). For example, hydrothermal fluids emitted at Clark volcano, Kermadec arc, and responsible for sea bed sulphate-sulphide mineralisation (dominated by barite, anhydrite and gypsum, or silica-Fe, with minor pyrite, sphalerite and galena), have been interpreted to be a mix of 40% sea water with K-rich lava-derived magmatic fluids (de Ronde et al. 2014). Bell (2016) has measured S isotopes of various sulphides at DeGrussa using SIMS, and found that texturally primary pyrite, pyrrhotite and chalcopyrite have relatively low $\delta^{34}S$ (mostly +1 – +7‰), whereas overprinting euhedral pyrite has $\delta^{34}S$ of +8.4 – +29.1‰. This raises the possibility of contamination of bulk analyses by secondary pyrite.

Significance of magnetite mineralisation and magnetite breccia

Massive magnetite mineralisation is not present in all VHMS deposits, although VHMS systems in volcano-sedimentary successions where the volcanic component is predominantly mafic (Besshi and Cyprus types) are associated with banded iron formation (Galley et al. 2007; Sebert et al. 2004; Lydon 1984; Hannington 2014). These distal chemical precipitates (exhalites) are believed to form by precipitation from sea floor hydrothermal plumes during the early stages of hydrothermal activity (Peter and Goodfellow 2003; Peter et al. 2007). In these deposits, magnetite is found together with finely layered quartz, magnetite, chlorite, Fe-carbonate, calcite and trace sulphides. Magnetite in these exhalites typically has high Mn (10^3–10^6 times sea water composition) and low Ti content (Peter and Goodfellow 2003; Dare et al. 2014). Magnetite is present in the Besshi-type Windy Craggy VHMS deposit of Canada, and intergrown magnetite and sulphide mineralisation has been described in the metamorphosed Cu-rich VHMS Fyre Lake deposit, Canada, and the Rudny-Altai, Russia, VHMS deposit (Sebert et al. 2004; Lobanov et al. 2014). Massive magnetite truncated by massive sulphide deposition has been described in Neoarchaean Cu-Zn VHMS deposits at Gossan Hill, Western Australia (Sharpe and Gemmell 2002). These authors interpreted this magnetite to have been deposited in the sub-surface, by sea water-derived hydrothermal fluids at $T > 300$ °C, low-fS_2 low-fO_2, and reducing conditions, and the occurrence of carbonate in this massive magnetite suggests the presence of CO_2 in the fluids. The spatially-restricted magnetite halo around the massive chalcopyrite, as well as an abundance of carbonate veins in magnetite overprinted by later brecciation, suggest that Red Bore mineralisation is likely to have formed in a similar scenario.

Brecciation of magnetite in the Red Bore ore may have been caused by sudden release of overpressured fluids, similarly to what is observed in hydrothermal systems associated with intrusions (hydrothermal breccia). This mechanism has been proposed for breccia intersected by drilling in hydrothermal sea floor systems in the Manus basin (Binns et al. 2007). Fluid release during short-lived events of magma instability associated with volcanic activity has also been proposed (e.g. Christopher et al. 2010). Alternatively, brecciation may be caused by other processes, such as tectonic movements along faults. Fault movements and fluid release would have likely been closely related in a volcanically and tectonically active setting (Richards 2013), such as the one believed to be responsible for the formation of the Narracoota Formation, so that distinguishing between different mechanisms may not be possible.

A mineralisation model for Red Bore and comparison with modern sea floor hydrothermal systems

The direct observation of modern submarine hydrothermal vents represents a unique way of testing genetic mechanisms for VHMS systems formed in the geological past. Drilling through one of these systems hosted in turbiditic sediments in the Juan de Fuca spreading centre has revealed the presence of a deep (200–210 m below sea bed), Cu-rich massive sulphide zone with 50 vol% sulphides and 8–16 wt% Cu that impregnated relatively coarse-grained clastic sediments (Zierenberg et al. 1998). This zone, termed deep copper zone (DCZ) extends horizontally underneath an impermeable silicified horizon, in contrast to the vertical vein-rich zone that directly underlies the deposits on the surface (as described

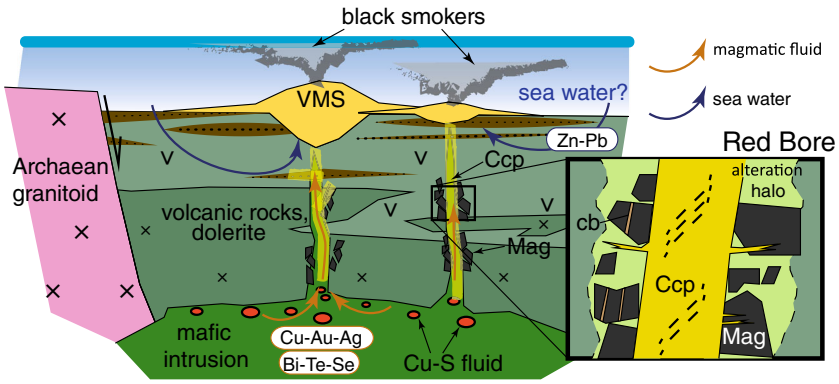

Fig. 10 A possible genetic model for the formation of Red Bore mineralised pipes and co-genetic VHMS deposits at DeGrussa. In this model, Cu, Au, Ag, Bi and other metals were transported from a magmatic fluid phase and fed into VHMS deposits at the surface, where they would have mixed with sea water-derived fluids. Other elements, such as Zn, are found in VHMS deposits but are depleted at Red Bore and may have been derived from leaching of the volcano-sedimentary succession by sea water-derived hydrothermal fluids

by Ohmoto 1996). These authors interpreted the DCZ as the lower part of a "feeder zone" to the hydrothermal system. Hardardóttir et al. (2009) have measured the composition of deep fluids in hydrothermal wells in Iceland, that were sampled at a depth of 1.3–1.5 km and temperature of 284–295 °C. These authors found high concentrations of metals (Fe 9–140 ppm, Zn 79–393 ppm, Cu 207–261 ppm, Pb 120–290 ppm), orders of magnitude higher than black smoker fluids, and interpreted this compositional difference as indicating substantial metal deposition at depth in this type of environments. These data may imply that an underappreciated deep metal deposition takes place in association with VHMS deposits.

These observations lead us to interpret the Red Bore mineralised pipes as being the result of sub-surface deposition during strongly focussed fluid flow, possibly along structural discontinuities. In our preferred model, the mineralisation represents the escape pathway for magmatic-hydrothermal fluids released by a mafic intrusion. As an alternative, leaching of volcanic rocks may also explain the narrow $\delta^{34}S$ and high Se, admitting low sulphate contribution from S-poor sea water in Palaeoproterozoic times. However, a model implying magmatic-derived fluids seems to better fit different pieces of evidence. The first stage of mineralisation included the deposition of massive magnetite along the fluid conduit by low-fS_2 fluids, with subsequent brecciation due to tectonic or hydrothermal processes. The trace element composition of magnetite at Red Bore falls in the "BIF" field of the Al + Mn vs. Ti + V plot (Fig. 7) and is akin to chemical precipitates that form banded iron formation in distal areas from submarine hydrothermal vents. Thus, fluids similar to the early Fe-rich S-poor fluids at Red Bore may have been responsible for deposition of banded iron formation, which is locally found in the Bryah Basin and are thought to be associated with sea floor hydrothermal systems (Peter and Goodfellow 2003). Massive chalcopyrite was subsequently deposited by S-Cu-Fe-rich fluids that exploited the same pathway. The anomalously high Cu concentrations at the centre of the mineralisation are compatible with deposition from a S-Cu-Fe-rich magmatic volatile phase similar to what described in mafic magma systems (Lowenstern et al. 1991; Yang and Scott 1996; Simon and Ripley 2011). Narrow ranges of S isotopic compositions ($\delta^{34}S \sim 0$ to +4 ‰), the presence of Bi-Te-Se-(Ag-Au) phases and the low concentrations of Zn and Pb in comparison with typical VHMS deposits are also compatible with a magmatic derivation of ore fluids with minor or no interaction with sea water (Fig. 10). Eventually, these fluids may have ascended towards the surface and contributed to the VHMS mineralisation known in the area (DeGrussa or similar VHMS deposits), which has lower Cu contents and has $\delta^{34}S$ extending towards higher values.

The Cu-Au association is typical of footwall mineralisation deposited from high temperature (300–350 °C) fluids or mineralisation at mid-oceanic ridges (Murphy and Meyer 1998; Galley et al. 2007). In these high-temperature fluids, Au is mostly interpreted to be transported as Cl complexes (Huston and Large 1989). However, others attribute Cu-Au mineralisation in sea floor mineralisation to the high-temperature oxidation of $Au(HS)_2^-$ (Hannington 2014).

In contrast to other sub-surface VHMS deposits where ore deposition occurred in stockwork-style veins and pores of permeable rocks (e.g. volcaniclastic rocks at Hercules South, Tasmania; Khin Zaw and Large 1992), the absence of open space-filling textures in our samples suggests that this type of depositional mechanism was not predominant at Red Bore. Instead, ore deposition at Red Bore occurred primarily by replacement, as shown by microtextures indicating sulfidation of precursor minerals (Fig. 3). Another

prominent difference between Red Bore mineralisation and Hercules South is the low Cu contents (< 1 wt%) of the latter, which is compatible with the low fluid temperatures estimated from fluid inclusion homogenisation temperatures (Khin Zaw and Large 1992).

Conclusions

The recent find at Red Bore prospect, Western Australia, includes elongate mineralisation several metres wide that has a zoned distribution of minerals: massive chalcopyrite at core (with Cu concentrations up to ~ 30 wt%) and brecciated massive magnetite at the margin. Mineralisation is hosted in Palaeoproterozoic mafic igneous rocks (mostly dolerite) and surrounded by a narrow talc-silica-carbonate alteration halo. In addition, disseminated sulphides intersected in proximity (hundreds of m) to the massive mineralisation is hosted by finely laminated mudrock. The mineralisation at Red Bore occurs in proximity to VHMS hosted sediments and mafic lavas at DeGrussa and the Cu-Ag-Au-rich composition of both deposits further supports a genetic relationship. However, the geometry of the mineralisation at Red Bore, the occurrence in shallow intrusive mafic rocks, as well as its mineralogical and trace element characteristics, set this mineralisation apart from associated VHMS deposits in the region and other VHMS systems worldwide. The mineralisation contains Ag and Au at hundreds and tens of ppm levels, respectively, and Bi, Te and Se at concentrations up to 100–1000 ppm. Gold is hosted in chalcopyrite, pyrite and in Bi-Te-(Se) phases, and no native Au was found. In situ S isotope analyses of pyrite and chalcopyrite indicate a narrow range of $\delta^{34}S$ (mostly +3.0 to +4.6‰), and $\Delta^{33}S \sim 0$. We interpret these mineralised bodies as having formed along strongly focussed pathways of fluid discharge, such as faults, along which S-rich fluids carried significant amounts of Cu, Fe, Au, Ag, Bi, Te and Se upwards towards the surface. Metals may have been derived from a degassing magma or from leaching of volcanic rocks. These fluids may have contributed to the overlying VHMS systems. Analyses of both Re-Os isotopes and Pb isotopes of sulphides at Red Bore indicate open-system behaviour, and support mixing of crustal Pb with highly radiogenic Pb.

Acknowledgments SIEF Science and Innovation Endowment Fund is acknowledged for funding this work. B. McDonald is thanked for assistance with LA-ICP-MS analysis. The authors would like to acknowledge the Australian Microscopy & Microanalysis Research Facility, AuScope, the Science and Industry Endowment Fund, and the State Government of Western Australian for contributing to the Ion Probe Facility at the Centre for Microscopy, Characterisation and Analysis at the University of Western Australia. This paper has benefited from reviews of D. Huston, Khin Zaw and G. Beaudoin.

References

Adamides NG (2010) Mafic-dominated volcanogenic sulphide deposits in the Troodos ophiolite, Cyprus part 2—a review of genetic models and guides for exploration. Applied. Earth Sci 119: 193–204

Agangi A, Reddy SM (2016) Open-system behaviour of magmatic fluid phase and transport of copper in arc magmas at Krakatau and Batur volcanoes, Indonesia. J Volcanol Geothermal Res 327:669–686. https://doi.org/10.1016/j.jvolgeores.2016.10.006

Bekker A, Barley ME, Fiorentini ML, Rouxel OJ, Rumble D, Beresford SW (2009) Atmospheric sulfur in Archean komatiite-hosted nickel deposits. Science 326(5956):1086–1089. https://doi.org/10.1126/science.1177742

Bell JM (2016) In situ multiple sulphur isotope analysis of the DeGrussa VHMS deposit: implications for exploration and mineralisation. Honours thesis, University of Western Australia, 56 p

Belousov I, Large RR, Meffre S, Danyushevsky LV, Steadman J, Beardsmore T (2016) Pyrite compositions from VHMS and orogenic Au deposits in the Yilgarn Craton, Western Australia: implications for gold and copper exploration. Ore Geol Rev 79:474–499. https://doi.org/10.1016/j.oregeorev.2016.04.020

Berkenbosch HA, de Ronde CEJ, Gemmell JB, McNeill AW, Goemann K (2012) Mineralogy and formation of black smoker chimneys from brothers submarine volcano, Kermadec arc. Econ Geol 107(8):1613–1633. https://doi.org/10.2113/econgeo.107.8.1613

Binns RA, Barriga FJAS, Miller DJ (2007) Leg 193 synthesis: anatomy of an active felsic-hosted hydrothermal system, eastern Manus Basin, Papua New Guinea. In: FJAS B, Binns RA, Miller DJ, Herzig PM (eds) Proc ODP, Sci Results, vol 193. Ocean Drilling Program, College Station, pp 1–71

Chen M, Campbell IH, Xue Y, Tian W, Ireland TR, Holden P, Cas RAF, Hayman PC, Das R (2015) Multiple sulfur isotope analyses support a magmatic model for the volcanogenic massive sulfide deposits of the Teutonic bore volcanic complex, Yilgarn craton, Western Australia. Econ Geol 110(6):1411–1423. https://doi.org/10.2113/econgeo.110.6.1411

Christopher T, Edmonds M, Humphreys MCS, Herd RA (2010) Volcanic gas emissions from Soufrière Hills volcano, Montserrat 1995-2009, with implications for mafic magma supply and degassing. Geophys Res Lett 37(19). https://doi.org/10.1029/2009GL041325

Ciobanu C, Cook NJ, Pring A (2005) Bismuth tellurides as gold scavengers mineral deposit research: meeting the global challenge. Springer, Berlin, pp 1383–1386

Ciobanu CL, Cook NJ, Damian F, Damian G (2006) Gold scavenged by bismuth melts: an example from alpine shear-remobilizates in the Highiş massif, Romania. Mineral Petrol 87:351–384

Cloutier J, Piercey SJ, Layne G, Heslop J, Hussey A, Piercey G (2015) Styles, textural evolution, and sulfur isotope systematics of Cu-rich sulfides from the Cambrian Whalesback volcanogenic massive sulfide deposit, central Newfoundland, Canada. Econ Geol 110:1215–1234

Dare SAS, Barnes S-J, Beaudoin G, Méric J, Boutroy E, Potvin-Doucet C (2014) Trace elements in magnetite as petrogenetic indicators. Mineral Deposita 49(7):785–796. https://doi.org/10.1007/s00126-014-0529-0

de Ronde CEJ, Hannington MD, Stoffers P, Wright IC, Ditchburn RG, Reyes AG, Baker ET, Massoth GJ, Lupton JE, Walker SL, Greene

RR, Soong CWR, Ishibashi J, Lebon GT, Bray CJ, Resing JA (2005) Evolution of a submarine magmatic-hydrothermal system: brothers volcano, southern Kermadec arc, New Zealand. Econ Geol 100(6):1097–1133. https://doi.org/10.2113/gsecongeo.100.6.1097

de Ronde CEJ, Walker SL, Ditchburn RG, Tontini FC, Hannington MD, Merle SG, Timm C, Handler MR, Wysoczanski RJ, Dekov VM, Kamenov GD, Baker ET, Embley RW, Lupton JE, Stoffers P (2014) The anatomy of a buried submarine hydrothermal system, Clark volcano, Kermadec arc, New Zealand. Econ Geol 109(8):2261–2292. https://doi.org/10.2113/econgeo.109.8.2261

Dora ML, Singh H, Kundu A, Shareef M, Randive KR, Joshi S (2014) Tsumoite (BiTe) and associated Ni-PGE mineralization from Gondpipri mafic-ultramafic complex, Bastar craton, Central India: mineralogy and genetic significance. Centr Eur J Geol 4:506–517

Drummond SE, Ohmoto H (1985) Chemical evolution and mineral deposition in boiling hydrothermal systems. Econ Geol 80(1):126–147. https://doi.org/10.2113/gsecongeo.80.1.126

Dupuis C, Beaudoin G (2011) Discriminant diagrams for iron oxide trace element fingerprinting of mineral deposit types. Mineral Deposita 46(4):319–335. https://doi.org/10.1007/s00126-011-0334-y

Farquhar J, Wu N, Canfield DE, Oduro H (2011) Connections between sulfur cycle evolution, sulfur isotopes, sediments, and base metal sulfide deposits. Econ Geol 105:509–533

Galley AG (2003) Composite synvolcanic intrusions associated with Precambrian VMS-related hydrothermal systems. Mineral Deposita 38(4):443–473. https://doi.org/10.1007/s00126-002-0300-9

Galley AG, Hannington M, Jonasson IR (2007) Volcanogenic massive sulphide deposits. In: Goodfellow WD (ed) Mineral deposits of Canada: a synthesis of major deposit-types, district metallogeny, the evolution of geological provinces, and exploration methods. Geol Assoc Canada, Mineral Deposits Division, Canada, pp 141–161

Gemmell JB, Sharpe R, Jonasson IR, Herzig PM (2004) Sulfur isotope evidence for magmatic contributions to submarine and subaerial gold mineralization: conical seamount and the Ladolam gold deposit, Papua New Guinea. Econ Geol 99(8):1711–1725. https://doi.org/10.2113/gsecongeo.99.8.1711

Hannington MD (2014) 13.18 - Volcanogenic massive sulfide deposits. In: Turekian HDHK (ed) Treatise on Geochemistry, 2nd edn. Elsevier, Oxford, pp 463–488

Hannington M, Herzig P, Scott S, Thompson G, Rona P (1991) Comparative mineralogy and geochemistry of gold-bearing sulfide deposits on the mid-ocean ridges. Mar Geol 101(1-4):217–248. https://doi.org/10.1016/0025-3227(91)90073-D

Hardardóttir V, Brown KL, Fridriksson T, Hedenquist JW, Hannington MD, Thorhallsson S (2009) Metals in deep liquid of the Reykjanes geothermal system, southwest Iceland: implications for the composition of seafloor black smoker fluids. Geology 37(12):1103–1106. https://doi.org/10.1130/G30229A.1

Hawke ML, Davidson GJ, Meffre S, Hilliard P, Large R, Gemmell JB (2015a) Geological evolution of the DeGrussa Cu-Au-Ag volcanic-hosted massive sulfide deposit, Western Australia. SEG 2015 conference. Hobart, Australia, Poster

Hawke ML, Meffre S, Stein H, Hilliard P, Large R, Gemmell JB (2015b) Geochronology of the DeGrussa volcanic-hosted massive sulphide deposit and associated mineralisation of the Yerrida, Bryah and Padbury basins, Western Australia. Precamb Res 267:250–284. https://doi.org/10.1016/j.precamres.2015.06.011

Heinrich CA, Ryan CG, Mernagh TP, Eadington PJ (1992) Segregation of ore metals between magmatic brine and vapor: a fluid inclusion study using PIXE microanalysis. Econ Geol 87(6):1566–1583. https://doi.org/10.2113/gsecongeo.87.6.1566

Henley RW, Mavrogenes J, Tanner D (2012) Sulfosalt melts and heavy metal (as-Sb-bi-Sn-Pb-Tl) fractionation during volcanic gas expansion: the el Indio (Chile) paleo-fumarole. Geofluids 12(3):199–215. https://doi.org/10.1111/j.1468-8123.2011.00357.x

Huston D, Relvas JRS, Gemmell JB, Drieberg S (2011) The role of granites in volcanic-hosted massive sulphide ore-forming systems: an assessment of magmatic–hydrothermal contributions. Mineral Deposita 46(5-6):473–507. https://doi.org/10.1007/s00126-010-0322-7

Huston DL, Pehrsson S, Eglington BM, Khin Zaw (2010) The geology and metallogeny of volcanic-hosted massive sulfide deposits: variations through geologic time and with tectonic setting. Econ Geol 105(3):571–591. https://doi.org/10.2113/gsecongeo.105.3.571

Huston DL, Large RR (1989) A chemical model for the concentration of gold in volcanogenic massive sulfide deposits. Ore Geol Rev 4(3):171–200. https://doi.org/10.1016/0169-1368(89)90017-6

Hynes A, Gee RD (1986) Geological setting and petrochemistry of the Narracoota Volcanics, Capricorn Orogen, Western Australia. Precamb Res 31(2):107–132. https://doi.org/10.1016/0301-9268(86)90070-7

Jamieson JW, Wing BA, Farquhar J, Hannington MD (2013) Neoarchaean seawater sulphate concentrations from sulphur isotopes in massive sulphide ore. Nat Geosci 6(1):61–64. https://doi.org/10.1038/ngeo1647

Kajiwara Y, Krouse HR (1971) Sulfur isotope partitioning in metallic sulfide systems. Can J Earth Sci 8(11):1397–1408. https://doi.org/10.1139/e71-129

Kamenetsky VS, Binns RA, Gemmell JB, Crawford AJ, Mernagh TP, Maas R, Steele D (2001) Parental basaltic melts and fluids in eastern Manus backarc basin: implications for hydrothermal mineralisation. Earth Planet Sci Lett 184(3-4):685–702. https://doi.org/10.1016/S0012-821X(00)00352-6

Keith M, Häckel F, Haase KM, Schwarz-Schampera U, Klemd R (2016) Trace element systematics of pyrite from submarine hydrothermal vents. Ore Geol Rev 72(Part 1):728–745

Khin Zaw, Large RR (1992) The precious metal-rich, South Hercules mineralization, western Tasmania; a possible subsea-floor replacement volcanic-hosted massive sulfide deposit. Econ Geol 87(3):931–952. https://doi.org/10.2113/gsecongeo.87.3.931

Large R, Doyle M, Raymond O, Cooke D, Jones A, Heasman L (1996) Evaluation of the role of Cambrian granites in the genesis of world class VHMS deposits in Tasmania. Ore Geol Rev 10(3-6):215–230. https://doi.org/10.1016/0169-1368(95)00024-0

Large RR (1992) Australian volcanic-hosted massive sulfide deposits; features, styles, and genetic models. Econ Geol 87(3):471–510. https://doi.org/10.2113/gsecongeo.87.3.471

Layton-Matthews D, Peter JM, Scott SD, Leybourne MI (2008) Distribution, mineralogy, and geochemistry of selenium in felsic volcanic-hosted massive sulfide deposits of the Finlayson Lake District, Yukon territory, Canada. Econ Geol 103(1):61–88. https://doi.org/10.2113/gsecongeo.103.1.61

Lehmann B, Zhao X, Zhou M, Du A, Mao J, Zeng P, Henjes-Kunst F, Heppe K (2013) Mid-Silurian back-arc spreading at the northeastern margin of Gondwana: the Dapingzhang dacite-hosted massive

sulfide deposit, Lancangjiang zone, southwestern Yunnan, China. Gondwana Res 24(2):648–663. https://doi.org/10.1016/j.gr.2012.12.018

Lobanov K, Yakubchuk A, Creaser RA (2014) Besshi-type VMS deposits of the Rudny Altai (Central Asia). Econ Geol 109(5):1403–1430. https://doi.org/10.2113/econgeo.109.5.1403

Lowenstern JB, Mahood GA, Rivers ML, Sutton SR (1991) Evidence for extreme partitioning of copper into a magmatic vapor-phase. Science 252(5011):1405–1409. https://doi.org/10.1126/science.252.5011.1405

Lydon JW (1984) Ore deposit models - 8. Volcanogenic massive suphide deposits. Part I: a descriptive model. Geosci Canada 11:195–202

Marcoux E, Moëlo Y, Leistel JM (1996) Bismuth and cobalt minerals as indicators of stringer zones to massive sulphide deposits, Iberian Pyrite Belt. Mineral Deposita 31:1–26

Marini L, Moretti R, Accornero M (2011) Sulfur isotopes in magmatic-hydrothermal systems, melts, and magmas. Rev Mineral Geochem 73(1):423–492. https://doi.org/10.2138/rmg.2011.73.14

Maslennikov VV, Maslennikova SP, Large RR, Danyushevsky LV, Herrington RJ, Stanley CJ (2013) Tellurium-bearing minerals in zoned sulfide chimneys from Cu-Zn massive sulfide deposits of the Urals, Russia. Mineral Petrol 107(1):67–99. https://doi.org/10.1007/s00710-012-0230-x

Moss R, Scott SD, Binns RA (2001) Gold content of eastern Manus Basin volcanic rocks: implications for enrichment in associated hydrothermal precipitates. Econ Geol 96:91–107

Murphy PJ, Meyer G (1998) A gold-copper association in ultramafic-hosted hydrothermal sulfides from the mid-Atlantic ridge. Econ Geol 93(7):1076–1083. https://doi.org/10.2113/gsecongeo.93.7.1076

Nadoll P, Angerer T, Mauk JL, French D, Walshe J (2014) The chemistry of hydrothermal magnetite: a review. Ore Geol Rev 61:1–32. https://doi.org/10.1016/j.oregeorev.2013.12.013

Occhipinti SA, Swager CP, Pirajno F (1998) Structural-metamorphic evolution of the Palaeoproterozoic Bryah and Padbury groups during the Capricorn orogeny, Western Australia. Precamb Res 90(3-4):141–158. https://doi.org/10.1016/S0301-9268(98)00046-1

Occhipinti SA, Sheppard S, Passchier C, Tyler IM, Nelson DR (2004) Palaeoproterozoic crustal accretion and collision in the southern Capricorn Orogen: the Glenburgh orogeny. Precamb Res 128(3-4):237–255. https://doi.org/10.1016/j.precamres.2003.09.002

Ohmoto H (1986) Stable isotope geochemistry of ore deposits. Rev Mineral Geochem 16:491–559

Ohmoto H (1996) Formation of volcanogenic massive sulfide deposits: the Kuroko perspective. Ore Geol Rev 10(3-6):135–177. https://doi.org/10.1016/0169-1368(95)00021-6

Peter JM, Goodfellow WD (2003) Hydrothermal sedimentary rocks of the heath Steele Belt, Bathurst mining camp, New Brunswick. 3. Application of hydrothermal sediment mineralogy and mineral and bulk composition to the exploration for concealed massive sulfide mineralization. In: Goodfellow WD, McCutcheon SR, Peter JM (eds) Massive sulphide deposits of the Bathurst mining camp, New Brunswick, and northern Maine, 11. Economic Geology, Monograph, pp 417–433

Peter JM, Layton-Matthews D, Piercey S, Bradshaw G, Paradis S, Boulton A (2007) Volcanic-hosted massive sulphide deposits of the Finlayson Lake District, Yukon. In: Goodfellow WD (ed) Mineral deposits of Canada: a synthesis of major deposit-types, district metallogeny, the evolution of geological provinces, and exploration methods. Geol Assoc Canada, Mineral Deposits Division, Canada, pp 471–508

Petersen S, Monecke T, Westhues A, Hannington MD, Gemmell JB, Sharpe R, Peters M, Strauss H, Lackschewitz K, Augustin N, Gibson H, Kleeberg R (2014) Drilling shallow-water massive sulfides at the Palinuro volcanic complex, Aeolian Island arc, Italy. Econ Geol 109(8):2129–2158. https://doi.org/10.2113/econgeo.109.8.2129

Pirajno F, Occhipinti SA (2000) Three Palaeoproterozoic basins-Yerrida, Bryah and Padbury-Capricorn Orogen, Western Australia. Aust J Earth Sci 47:675–688

Pirajno F, Occhipinti SA, Swager CP (2000) Geology and mineralisation of the Palaeoproterozoic Bryah and Padbury basins Western Australia. Geol Surv Western Australia, Dept Minerals Energy, 52 p

Pirajno F, Jones JA, Hocking RM, Halilovic J (2004) Geology and tectonic evolution of Palaeoproterozoic basins of the eastern Capricorn Orogen, Western Australia. Precamb Res 128(3-4):315–342. https://doi.org/10.1016/j.precamres.2003.09.006

Pirajno F, Chen Y, Li N, Li C, L-m Z (2016) Besshi-type mineral systems in the Palaeoproterozoic Bryah Rift-Basin, Capricorn Orogen, Western Australia: implications for tectonic setting and geodynamic evolution. Geosci Front 7(3):345–357. https://doi.org/10.1016/j.gsf.2015.09.003

Reddy SM, Occhipinti SA (2004) High-strain zone deformation in the southern Capricorn Orogen, Western Australia: kinematics and age constraints. Precamb Res 128(3-4):295–314. https://doi.org/10.1016/j.precamres.2003.09.005

Richards JP (2013) Giant ore deposits formed by optimal alignments and combinations of geological processes. Nat Geosci 6(11):911–916. https://doi.org/10.1038/ngeo1920

Ripley EM, Li C (2003) Sulfur isotope exchange and metal enrichment in the formation of magmatic Cu-Ni-(PGE) deposits. Econ Geol 98(3):635–641. https://doi.org/10.2113/gsecongeo.98.3.635

Ross P-S, Mercier-Langevin P (2014) Igneous rock associations 14. The volcanic setting of VMS and SMS deposits: A review. Geosci Canada 41(3)

Sabir H (1980) Metallogenic and textural features of sulfide mineralization at Jabal Sayid (Saudi Arabia). Bulletin du Bureau de Recherches Geologiques et Minieres Serie 2, Section II: 103–111

Sandfire Resources Report (2016) DeGrussa mine plan, mineral resource and ore reserve update. www.sandfire.com.au

Sebert C, Hunt J, Foreman IJ (2004) Geology and lithogeochemistry of the Fyre Lake copper-cobalt-gold sulphide-magnetite deposit, southeastern Yukon Yukon Geological Survey Open file 2004–17. pp 46

Shanks WC III (2001) Stable isotopes in seafloor hydrothermal systems: vent fluids, hydrothermal deposits, hydrothermal alteration, and microbial processes. Rev Mineral Geochem 43(1):469–525. https://doi.org/10.2138/gsrmg.43.1.469

Shanks III WC (2012) Hydrothermal alteration in volcanogenic massive sulfide occurrence model. US Geol Surv Sci Invest Report 2010–5070 –C. 12 p

Sharpe R, Gemmell JB (2002) The Archean cu-Zn magnetite-rich Gossan Hill volcanic-hosted massive sulfide deposit, Western Australia: genesis of a multistage hydrothermal system. Econ Geol 97(3):517–539. https://doi.org/10.2113/gsecongeo.97.3.517

Simon AC, Ripley EM (2011) The role of magmatic sulfur in the formation of ore deposits. Rev Mineral Geochem 73(1):513–578. https://doi.org/10.2138/rmg.2011.73.16

Solomon M, Gemmell JB, Khin Zaw (2004) Nature and origin of the fluids responsible for forming the Hellyer Zn–Pb–Cu, volcanic-hosted massive sulphide deposit, Tasmania, using

fluid inclusions, and stable and radiogenic isotopes. Ore Geol Rev 25(1-2):89–124. https://doi.org/10.1016/j.oregeorev.2003.11.001

Stacey JS, Kramers JD (1975) Approximation of terrestrial lead isotopic evolution by a two-stage model. Earth Planet Sci Lett 26(2):207–221. https://doi.org/10.1016/0012-821X(75)90088-6

Sun W, Arculus RJ, Kamenetsky VS, Binns RA (2004) Release of gold-bearing fluids in convergent margin magmas prompted by magnetite crystallization. Nature 431(7011):975–978. https://doi.org/10.1038/nature02972

Symonds RB, Rose WI, Reed MH, Lichte FE, Finnegan DL (1987) Volatilization, transport and sublimation of metallic and non-metallic elements in high temperature gases at Merapi volcano, Indonesia. Geochim Cosmochim Acta 51(8):2083–2101. https://doi.org/10.1016/0016-7037(87)90258-4

Timm C, de Ronde CEJ, Leybourne MI, Layton-Matthews D, Graham IJ (2012) Sources of chalcophile and siderophile elements in Kermadec arc lavas. Econ Geol 107(8):1527–1538. https://doi.org/10.2113/econgeo.107.8.1527

Urabe T, Marumo K (1991) A new model for Kuroko-type deposits of Japan. Episodes 14:246–251

Wohlgemuth-Ueberwasser CC, Viljoen F, Petersen S, Vorster C (2015) Distribution and solubility limits of trace elements in hydrothermal black smoker sulfides: an in-situ LA-ICP-MS study. Geochim Cosmochim Acta 159:16–41. https://doi.org/10.1016/j.gca.2015.03.020

Yang K, Scott SD (1996) Possible contribution of a metal-rich magmatic fluid to a sea-floor hydrothermal system. Nature 383(6599):420–423. https://doi.org/10.1038/383420a0

Yeats CJ, Parr JM, Binns RA, Gemmell JB, Scott SD (2014) The SuSu knolls hydrothermal field, eastern Manus basin, Papua New Guinea: an active submarine high-sulfidation copper-gold system. Econ Geol 109(8):2207–2226. https://doi.org/10.2113/econgeo.109.8.2207

Zierenberg RA, Fouquet Y, Miller DJ, Bahr JM, Baker PA, Bjerkgard T, Brunner CA, Duckworth RC, Gable R, Gieskes J, Goodfellow WD, Groschel-Becker HM, Guerin G, Ishibashi J, Iturrino G, James RH, Lackschewitz KS, Marquez LL, Nehlig P, Peter JM, Rigsby CA, Schultheiss P, Shanks WC, Simoneit BRT, Summit M, Teagle DAH, Urbat M, Zuffa GG (1998) The deep structure of a sea-floor hydrothermal deposit. Nature 392(6675):485–488. https://doi.org/10.1038/33126